

Lightweight and Adaptive FDD Massive MIMO CSI Feedback with Deep Equilibrium Learning

Yifan Ma*, Wentao Yu*, Xianghao Yu*, Jun Zhang*, Shenghui Song*[†], and Khaled B. Letaief*

*Dept. of ECE, The Hong Kong University of Science and Technology, Hong Kong

[†]Division of ISD, The Hong Kong University of Science and Technology, Hong Kong

Email: *{ymabj, wyuaq, eexyu, eejzhang, eeshsong, eekhaled}@ust.hk

Abstract—In frequency-division duplexing (FDD) massive multiple-input multiple-output (MIMO) systems, downlink channel state information (CSI) needs to be sent from users back to the base station (BS), which causes prohibitive feedback overhead. In this paper, we propose a lightweight and adaptive deep learning-based CSI feedback scheme by capitalizing on deep equilibrium models. Different from existing deep learning-based approaches that stack multiple explicit layers, we propose an implicit equilibrium block to mimic the process of an infinite-depth neural network. In particular, the implicit equilibrium block is defined by a fixed-point iteration and the trainable parameters in each iteration are shared, which results in a lightweight model. Furthermore, the number of forward iterations can be adjusted according to the users' computational capability, achieving an online accuracy-efficiency trade-off. Simulation results will show that the proposed method obtains a comparable performance as the existing benchmarks but with much-reduced complexity and permits an accuracy-efficiency trade-off at runtime.

I. INTRODUCTION

Massive multiple-input multiple-output (MIMO) systems are regarded as a key enabler for 5G and beyond wireless communication systems [1] where frequency-division duplexing (FDD) is considered a compelling operation mode [2]. In FDD massive MIMO systems, users need to compress and feed the downlink channel state information (CSI) back to the base station (BS) to facilitate potential beamforming gain. However, the CSI dimension increases significantly as the size of the BS antenna array keeps expanding, which causes prohibitive feedback overhead. Conventional compressive sensing (CS) methods were widely applied for the CSI compression and recovery task [3], but they suffered from noteworthy limitations, such as the ideal assumption of channel sparsity, ability to exploit the channel structures, and high computational cost of the iterative operations [4].

Thanks to the recent success of deep learning, the learning-based auto-encoder and decoder structure can be leveraged to effectively compress and reconstruct downlink CSI. The exploratory work [4] proposed a convolutional neural network (CNN)-based CsiNet which outperforms the CS-based algorithms especially at low compression ratios. Many subsequent studies including ConvCsiNet in [5] and TransNet in [6] aimed to further improve feedback accuracy using deeper CNNs and attention mechanism, respectively. However, the performance improvement is at the cost of the neural network complexity. For example, the floating point operation (FLOP) number of ConvCsiNet is almost one hundred times that of CsiNet. This

will put prohibitive burdens on memory and computational consumption, making the deployment of these deep learning-based designs challenging in practice.

To reduce the huge execution cost, various lightweight feedback schemes were proposed. Efficient neural network architectures were designed by replacing redundant neural network layers with simplified compositions. For example, the vanilla convolutional layers were replaced with shuffle layers in [5] to achieve a comparable accuracy when the number of FLOPs is 1/3 of ConvCsiNet. However, existing models can not fit the dynamic communication environment. In practice, the computational budget varies (e.g., numerous background applications can reduce the available computation capability) and the energy budget differs (e.g., a mobile phone may be in the power-saving mode). As such, different models need to be pre-trained, stored, and allocated to different devices/situations according to the resource budget, leading to large memory and time cost. Hence, it is of great value to develop new models that provide a flexible trade-off between accuracy and efficiency.

In this paper, we propose a lightweight and adaptive CSI feedback scheme for FDD massive MIMO systems, permitting an instant accuracy-efficiency trade-off at runtime. In particular, instead of stacking multiple well-designed *explicit* layers, i.e., the output is computed by explicitly cascading a series of nonlinear mappings, we develop a learning model with *implicit* equilibrium blocks. Specifically, the equilibrium block specifies the input-output relationship by a fixed-point equation. The forward propagation is a fixed-point finding process, which is separated from the backward neural network training, making the backpropagation only consume a constant memory [7]. Besides, the trainable parameters in different iterations are shared, which results in a lightweight model. Given that the computational capability is typically limited at the user side, the number of implicit iterations at the users is adjusted according to latency and computational budget during the inference stage. At the BS side, we apply an efficient solver to generate the output of the equilibrium block, which is equivalent to running an infinite-depth explicit neural network. It is shown through extensive simulation results that the proposed method outperforms the conventional CsiNet [4] and has a comparable or even better performance than the existing lightweight approach [5] with greatly reduced complexity.

Notations: x is a scalar, \mathbf{x} is a vector, and \mathbf{X} denotes a matrix. Let \mathbf{X}^T and \mathbf{X}^H denote the transpose and conjugate transpose of matrix \mathbf{X} , respectively. \mathbf{I} stands for an identity matrix. $\|\mathbf{X}\|_2$ and \mathbf{X}^{-1} denote the Frobenius norm and the inverse of matrix \mathbf{X} , respectively. $\mathbb{E}\{\cdot\}$ denotes the statistical expectation. f_θ denotes a mapping parameterized by learnable parameters θ . $\mathbf{X}^{[t]}$ represents the value of \mathbf{X} in the t -th iteration and \mathbf{X}^* represents the fixed-point. $\mathbb{C}^{m \times n}$ is the set of all $m \times n$ complex-valued matrices.

II. SYSTEM MODEL AND PROBLEM FORMULATION

This work considers a single-cell FDD massive MIMO system where the BS is equipped with N_t transmit antennas and the user is equipped with a single receive antenna. For ease of illustration, a single user case is considered while the proposed scheme can be easily generalized to the multi-user case. An orthogonal frequency division multiplexing (OFDM) system with N_c subcarriers is considered. The received signal on the n -th subcarrier is expressed as

$$y_n = \mathbf{h}_n^H \mathbf{v}_n x_n + z_n, \quad (1)$$

where $\mathbf{h}_n \in \mathbb{C}^{N_t \times 1}$, $\mathbf{v}_n \in \mathbb{C}^{N_t \times 1}$, $x_n \in \mathbb{C}$, and $z_n \in \mathbb{C}$ denote the downlink channel vector, downlink beamforming vector, the transmit symbol, and the additive noise of the n -th subcarrier, respectively. The CSI matrix of all subcarriers in the spatial-frequency domain is thus denoted by $\mathbf{H} = [\mathbf{h}_1, \dots, \mathbf{h}_{N_c}]^H \in \mathbb{C}^{N_c \times N_t}$. The downlink beamforming design requires the BS to know information about the downlink channel. However, the channel matrix \mathbf{H} contains $2N_c N_t$ real elements and the feedback overhead is prohibitive for FDD massive MIMO system. In this paper, we assume that the downlink channel is perfectly known at the user side via pilot-based training and focus on the efficient feedback design [4]–[6].

Note that \mathbf{H} can be sparsified in the angular-delay domain using a 2D discrete Fourier transform (2D-DFT) [4] as follows

$$\mathbf{H}' = \mathbf{F}_d \mathbf{H} \mathbf{F}_a, \quad (2)$$

where $\mathbf{F}_d \in \mathbb{C}^{N_c \times N_c}$ and $\mathbf{F}_a \in \mathbb{C}^{N_t \times N_t}$ are two DFT matrices. The matrix \mathbf{H}' is sparse due to the scattering environment. Only the first N_a rows of \mathbf{H}' contain significant values and other elements are close to zero because the time delay between multipath arrivals is within a limited period [4]. Therefore, we keep the first N_a rows of \mathbf{H}' ($N_a < N_c$) and obtain $\mathbf{H}'' \in \mathbb{C}^{N_a \times N_t}$. By doing this, we can compress \mathbf{H}'' instead of \mathbf{H} with only $2N_a N_t$ entries and imperceptible information loss.

In this work, the deep learning-based method is adopted for CSI compression and recovery. The encoding process at the user side is given by

$$\mathbf{s} = \mathcal{E}_{\theta_e}(\mathbf{H}''), \quad (3)$$

which transforms the channel matrix into an M -length codeword \mathbf{s} . The parameterized mapping $\mathcal{E}_{\theta_e}(\cdot)$ denotes the compression procedure and θ_e is the trainable parameters in the encoder. The compression ratio is defined as $\gamma = M/2N_a N_t$. We use the same setting as [4]–[6] where \mathbf{s} is assumed to be

sent back to the BS via error-free transmission. After receiving the codeword, the BS reconstructs the channel matrix through a decoder, expressed as

$$\hat{\mathbf{H}}'' = \mathcal{D}_{\theta_d}(\mathbf{s}), \quad (4)$$

where $\mathcal{D}_{\theta_d}(\cdot)$ denotes the recovery procedure and θ_d represents the trainable parameters at the decoder. The objective is to minimize the mean squared error (MSE) between the recovered channel and the true channel, given by

$$\min_{\theta_e, \theta_d} \mathbb{E} \{ \|\mathbf{H}'' - \mathcal{D}_{\theta_d}(\mathcal{E}_{\theta_e}(\mathbf{H}''))\|_2^2 \}. \quad (5)$$

The mapping $\mathcal{E}_{\theta_e}(\cdot)$ and $\mathcal{D}_{\theta_d}(\cdot)$ can be instantiated as auto-encoder and decoder, and can be jointly trained via end-to-end learning [4]–[6]. However, most of the existing works improve the reconstruction accuracy at the expense of high neural network complexity, which is not affordable for mobile devices due to limited resources. Moreover, the existing feedback schemes lack a performance-complexity trade-off during execution. In practice, different devices have different runtime for a neural network [8]. Given the same latency budget, high-end devices can achieve better performance by running complicated models, while low-end ones have to sacrifice accuracy to meet the response time constraint. Even for the same device, the resource availability varies under different situations. Therefore, it is of vital importance to design a lightweight and adaptive CSI feedback scheme.

III. PROPOSED CSI FEEDBACK SCHEME WITH DEEP EQUILIBRIUM LEARNING

In this section, we present the overall diagram of the proposed deep equilibrium learning-based CSI feedback scheme, delicate design of the encoding and decoding blocks, and training strategies.

A. Overall Structure

The widely adopted explicit deep neural network model can be written as

$$\mathbf{y}_{\text{out}}^{[i+1]} = f_\theta^{[i+1]}(\mathbf{y}_{\text{out}}^{[i]}; \mathbf{x}_{\text{in}}), \quad i = 0, 1, \dots, L-1, \quad (6)$$

where $\mathbf{y}_{\text{out}}^{[i]}$ is the output of the i -th layer, $f_\theta^{[i]}$ represents the i -th layer's parameterized function, \mathbf{x}_{in} denotes the input, and L is the number of layers. Recent surprising findings in [9] showed that employing the same transformation function in each layer still leads to competitive results. The shared-weight neural network is correspondingly expressed as

$$\mathbf{y}_{\text{out}}^{[i+1]} = f_\theta(\mathbf{y}_{\text{out}}^{[i]}; \mathbf{x}_{\text{in}}), \quad i = 0, 1, \dots, L-1, \quad (7)$$

and thus the number of trainable parameters is greatly reduced. Note that stacking an infinite number of shared-weight layers corresponds to finding the fixed-point solution of the equation [7], [10]

$$\mathbf{y}_{\text{out}}^* = f_\theta(\mathbf{y}_{\text{out}}^*; \mathbf{x}_{\text{in}}). \quad (8)$$

In the implicit equilibrium model, it allows us to directly find the equilibrium point $\mathbf{y}_{\text{out}}^*$ with an off-the-shelf solver instead of iteratively performing $f_\theta(\cdot)$. Besides, thanks to the implicit function theorem, the backward propagation is independent of

the black-box fixed-point solver, making the trainable weight update equivalent to one single layer. These advantages of deep equilibrium learning inspire multiple applications including natural language processing [7] and computer vision [11].

With the same trainable parameters in each iteration, the output and all hidden units of conventional deep equilibrium learning should have the same dimensions. For the CSI compression and recovery task, the input channel matrix needs to be downsampled and upsampled to guarantee $M \ll 2N_a N_t$. Hence, it is not feasible if we only apply equilibrium blocks for the mappings in (3) and (4). Furthermore, the computational capability of mobile users is generally limited, which requires a simple yet effective encoder to be deployed at the user side. Based on these two aspects, we incorporate the implicit equilibrium block with traditional explicit neural network design. The overall diagram is shown in Fig. 1 and the operations at the test stage are summarized in **Algorithm 1**.

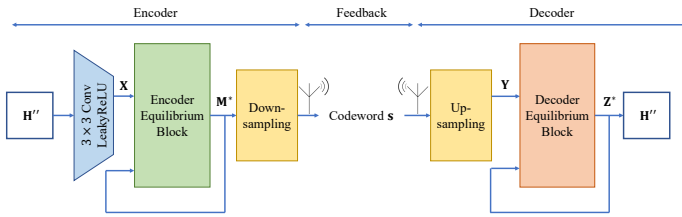


Fig. 1. Diagram of the proposed implicit layer-based CSI feedback scheme.

Algorithm 1 Inference Stage of the Proposed CSI Feedback Scheme with Deep Equilibrium Learning

- 1: **Input:** Truncated channel matrix in angular-delay domain \mathbf{H}'' . Error tolerance ϵ_e , ϵ_d , and maximum iteration number T_e , T_d of the encoding and decoding blocks, respectively. Well-trained encoding block f_{pre} , f_{eim} , and f_{down} . Well-trained decoding block f_{up} and f_{dim} . Limited-memory Broyden's fixed-point solver g_{solv} .
 - 2: **Output:** Estimated channel matrix $\hat{\mathbf{H}}''$
 - 3: **Initialize:** $\mathbf{M}^{[0]} \leftarrow \mathbf{0}$, $t \leftarrow 0$, and $\mathbf{Z}^{[0]} \leftarrow \mathbf{0}$
 - 4: **Encoder:**
 - 5: $\mathbf{X} \leftarrow f_{\text{pre}}(\mathbf{H}'')$;
 - 6: **repeat**
 - 7: $\mathbf{M}^{[t+1]} \leftarrow f_{\text{eim}}(\mathbf{M}^{[t]}, \mathbf{X})$;
 - 8: $t \leftarrow t + 1$;
 - 9: **until** $\|\mathbf{M}^{[t]} - \mathbf{M}^{[t-1]}\|_2 < \epsilon_e$ or $t > T_e$
 - 10: $\mathbf{s} \leftarrow f_{\text{down}}(\mathbf{M}^{[t]})$;
 - 11: **Decoder:**
 - 12: $\mathbf{Y} \leftarrow f_{\text{up}}(\mathbf{s})$;
 - 13: $\hat{\mathbf{H}}'' \triangleq \mathbf{Z}^* \leftarrow g_{\text{solv}}(f_{\text{dim}}, \mathbf{Z}^{[0]}, \epsilon_d, T_d)$;
-

Mathematically, the encoding process is expressed as

$$\begin{aligned} \mathbf{X} &= f_{\text{pre}}(\mathbf{H}''), \\ \mathbf{M}^{[t]} &= f_{\text{eim}}(\mathbf{M}^{[t-1]}, \mathbf{X}), \quad t = 1, \dots, T_e \\ \mathbf{s} &= f_{\text{down}}(\mathbf{M}^*). \end{aligned} \quad (9)$$

$f_{\text{pre}}(\cdot)$ is the preprocessing block to form the input injection \mathbf{X} . The input injection is pivotal to equilibrium models. Since

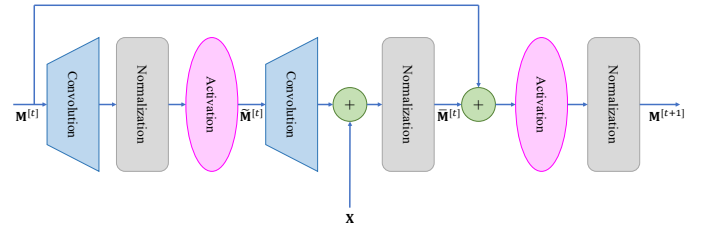


Fig. 2. The encoder-side implicit equilibrium block.

the fixed-point \mathbf{M}^* does not depend on any initial value of $\mathbf{M}^{[0]}$, preprocessing \mathbf{H}'' and injecting \mathbf{X} properly ensures the dependency between the fixed-point and the model input. $f_{\text{eim}}(\cdot, \cdot)$ denotes the encoder-side implicit equilibrium block. During the training stage, the forward fixed-point solution is calculated via an existing solver. In the test stage, due to insufficient computational resources of devices, the implicit equilibrium block is terminated with an error threshold ϵ_e and a maximum number of iterations T_e , whichever reaches first. Note that the hyperparameters ϵ_e and T_e can be adjusted flexibly during runtime according to the resource budget. Therefore, it provides us with an adaptive CSI feedback scheme executable in different scenarios without additional training or model downloading costs. The output of the implicit model \mathbf{M}^* is then fed into the downsampling block $f_{\text{down}}(\cdot)$ which reduces the output into M dimensions. The codeword \mathbf{s} is then transmitted back to the BS.

At the BS side, the decoding process is given by

$$\begin{aligned} \mathbf{Y} &= f_{\text{up}}(\mathbf{s}), \\ \mathbf{Z}^* &= \underbrace{f_{\text{dim}} \circ \dots \circ f_{\text{dim}}}_{\text{until convergence}}(\mathbf{Z}^{[0]}, \mathbf{Y}) \\ &= g_{\text{solv}}(f_{\text{dim}}, \mathbf{Z}^{[0]}, \epsilon_d, T_d), \\ \hat{\mathbf{H}}'' &= \mathbf{Z}^*, \end{aligned} \quad (10)$$

where $f_{\text{up}}(\cdot)$ represents the upsampling block, \mathbf{Y} is the input injection of the decoder-side implicit equilibrium block $f_{\text{dim}}(\cdot, \cdot)$, $\mathbf{Z}^{[0]}$ is the initial value, and g_{solv} denotes an existing fixed-point solver with a predetermined error tolerance ϵ_d and a maximum number of iterations T_d . The powerful computation capability of BS allows us to obtain a fixed-point solution of $f_{\text{dim}}(\cdot, \cdot)$ with higher accuracy. At both the training and inference stages, the output of the decoder-side implicit equilibrium module is computed by g_{solv} , which will be discussed in the following subsection.

B. Design of Encoding and Decoding Blocks

1) **Encoder:** The input to the encoder is the real and imaginary part of \mathbf{H}'' , forming a $2 \times N_a \times N_t$ dimensional tensor. The preprocessing module of the encoder, i.e., $f_{\text{pre}}(\cdot)$, is constructed by 3×3 convolutional kernels followed by LeakyReLU activation functions. This module effectively extracts the information from the input CSI matrix and fuses the features from both the real and imaginary parts at an affordable cost. The output of the preprocessing module is treated as the input injection to the implicit equilibrium block. The major

component of the equilibrium module is the transformation $f_{\text{eim}}(\cdot, \cdot)$. Inspired by the residual network [12], the identity shortcut connections are introduced, as shown in Fig. 2. Mathematically, the encoder-side equilibrium block is given by

$$\begin{aligned}\widetilde{\mathbf{M}}^{[t]} &= \text{ReLU}(\text{GroupNorm}(\text{Conv}(\mathbf{M}^{[t]}))), \\ \bar{\mathbf{M}}^{[t]} &= \text{GroupNorm}(\text{Conv}(\widetilde{\mathbf{M}}^{[t]} + \mathbf{X})), \\ \mathbf{M}^{[t+1]} &= \text{GroupNorm}(\text{ReLU}(\bar{\mathbf{M}}^{[t]} + \mathbf{M}^{[t]})).\end{aligned}\quad (11)$$

The 3×3 kernels are used for two convolution operations $\text{Conv}(\cdot)$ with the internal channel number being two times the input channel number. Group normalization is adopted as the normalization procedure to stabilize training [13]. The initial value of the latent variable $\mathbf{M}^{[0]}$ is set to be all zeros with the same dimension as \mathbf{X} . After the equilibrium module, the last downsampling block in the encoder is implemented by consecutive 2-stride 3×3 convolutions.

During the forward pass of training, to compute the fixed-point \mathbf{M}^* , we first rewrite $\mathbf{M}^* = f_{\text{eim}}(\mathbf{M}^*, \mathbf{X})$ into

$$h_{\text{eim}}(\mathbf{M}^*, \mathbf{X}) = f_{\text{eim}}(\mathbf{M}^*, \mathbf{X}) - \mathbf{M}^* = 0. \quad (12)$$

To find the root of (12), a natural choice is Newton's method

$$\mathbf{M}^{[i+1]} = \mathbf{M}^{[i]} - (J_{h_{\text{eim}}|\mathbf{M}^{[i]}}^{-1})h_{\text{eim}}(\mathbf{M}^{[i]}, \mathbf{X}), \quad \mathbf{M}^{[0]} = \mathbf{0}.$$

However, since the required storage and computation for calculating $J_{h_{\text{eim}}|\mathbf{M}^{[i]}}^{-1}$ are expensive, we use a limited-memory Broyden's method [11]

$$\mathbf{M}^{[i+1]} = \mathbf{M}^{[i]} - \alpha \mathbf{B}^{[i]} h_{\text{eim}}(\mathbf{M}^{[i]}, \mathbf{X}), \quad \mathbf{M}^{[0]} = \mathbf{0},$$

where α is step size and $\mathbf{B}^{[i]}$ is a low-rank approximation of $J_{h_{\text{eim}}|\mathbf{M}^{[i]}}^{-1}$ which is constructed by

$$\mathbf{B}^{[i+1]} = \mathbf{B}^{[0]} + \sum_{k=1}^i \mathbf{u}^{[k]} \mathbf{v}^{[k]T} = \mathbf{B}^{[0]} + \mathbf{U} \mathbf{V}^T, \quad (13)$$

where \mathbf{u} and \mathbf{v} come from the Sherman-Morrison formula [11] and $\mathbf{B}^{[0]}$ is initialized by $-\mathbf{I}$. To restrict the memory consumption, no more than K low-rank updates \mathbf{u} , \mathbf{v} are stored. In the backward pass of training, conventional explicit deep learning has to go through the iterations in the limited-memory Broyden's method to compute the gradient. In contrast, in the proposed deep equilibrium learning, we can directly backpropagate using the Jacobian of h_{eim} at \mathbf{M}^* , i.e.,

$$\begin{aligned}\frac{\partial \ell}{\partial \theta} &= \frac{\partial \ell}{\partial \mathbf{M}^*} (-J_{h_{\text{eim}}|\mathbf{M}^*}^{-1}) \frac{\partial f_{\text{eim}}(\mathbf{M}^*, \mathbf{X})}{\partial \theta}, \\ \frac{\partial \ell}{\partial \mathbf{X}} &= \frac{\partial \ell}{\partial \mathbf{M}^*} (-J_{h_{\text{eim}}|\mathbf{M}^*}^{-1}) \frac{\partial f_{\text{eim}}(\mathbf{M}^*, \mathbf{X})}{\partial \mathbf{X}},\end{aligned}\quad (14)$$

where ℓ denotes the training loss and θ denotes the trainable parameters. The proof is based on the implicit function theorem and is shown in [7]. By doing this, we separate the forward fixed-point finding procedures from the backward neural network training. The backpropagation is thus based on differentiating through one layer at the fixed-point, i.e., $\frac{\partial f_{\text{eim}}(\mathbf{M}^*, \mathbf{X})}{\partial \theta}$ and $\frac{\partial f_{\text{eim}}(\mathbf{M}^*, \mathbf{X})}{\partial \mathbf{X}}$. No intermediate values in the infinite-depth equilibrium block are required and the training memory consumption is constant, which is equivalent to

Algorithm 2 Training Stage of the Proposed CSI Feedback Scheme with Deep Equilibrium Learning

- 1: **Input:** Truncated channel matrix in angular-delay domain \mathbf{H}'' forms the training dataset. Error tolerance ϵ_e , ϵ_d , and maximum iteration number T_e , T_d of the encoding and decoding blocks, respectively. Encoding blocks f_{pre} , f_{eim} , and f_{down} , and decoding blocks f_{up} and f_{dim} with Kaiming initialization [14]. Limited-memory Broyden's fixed-point solver g_{solv} . Number of maximum training epoch I_{max} .
 - 2: **Output:** Well-trained learning model.
 - 3: **Initialize:** $\mathbf{M}^{[0]} \leftarrow \mathbf{0}$, $i \leftarrow 0$, and $\mathbf{Z}^{[0]} \leftarrow \mathbf{0}$
 - 4: **repeat**
 - 5: **Forward pass:**
 - 6: $\mathbf{X} \leftarrow f_{\text{pre}}(\mathbf{H}'')$;
 - 7: $\mathbf{M}^* \leftarrow g_{\text{solv}}(f_{\text{eim}}, \mathbf{M}^{[0]}, \epsilon_e, T_e)$;
 - 8: $\mathbf{s} \leftarrow f_{\text{down}}(\mathbf{M}^*)$;
 - 9: $\mathbf{Y} \leftarrow f_{\text{up}}(\mathbf{s})$;
 - 10: $\hat{\mathbf{H}}'' \triangleq \mathbf{Z}^* \leftarrow g_{\text{solv}}(f_{\text{dim}}, \mathbf{Z}^{[0]}, \epsilon_d, T_d)$;
 - 11: **Backward pass:**
 - 12: Compute the gradient according to (14). Apply mini-batch stochastic gradient descent to update the trainable parameters.
 - 13: $i \leftarrow i + 1$;
 - 14: **until** The loss function in the validation set converges or $i > I_{\text{max}}$.
-

training a one-layer neural network. The inverse of Jacobians can also be computed with the low-rank approximation (13) by limited-memory Broyden's method.

In the inference stage, we manually set the maximum iteration of the encoder equilibrium module according to the resource budget. Notice that truncated encoder implicit residual iterations only lead to imperceptible performance loss empirically, demonstrating the superiority of the proposed scheme in terms of flexibility.

2) *Decoder:* Given the powerful computational resources at the BS, it can support more complicated operations than the users and thus improve the overall reconstruction accuracy. The upsampling operations at the decoder are implemented by bilinear interpolation followed by 3×3 convolutions. The upsampling block $f_{\text{up}}(\cdot)$ recovers the codeword \mathbf{s} to the original CSI matrix dimension and finishes a preliminary reconstruction. After the upsampling module, we adopt a decoder-side implicit equilibrium block, whose structure is the same as in Fig. 2. The input injection to the decoder-side implicit equilibrium block is the output of the upsampling block and $\mathbf{Z}^{[0]}$ is initialized by all zeros. It is shown that for a lower compression ratio, i.e., γ is smaller and M is limited, larger kernel size will provide better performance. Moreover, the activation function also plays an important role in complicated neural network design and Swish has shown its advantages over ReLU in deeper networks [15], expressed as

$$\text{Swish}(x) = x \cdot \text{Sigmoid}(x) = x \cdot \frac{1}{1 + e^{-x}}. \quad (15)$$

Therefore, different from the encoder, we adopt 5×5 kernel as convolution operation and employ $\text{Swish}(\cdot)$ as the activation function in the decoder-side implicit module. The fixed-point \mathbf{Z}^* is also acquired via limited-memory Broyden's method at both the training and test stages. The training stage of the proposed deep equilibrium learning-based method is summarized in **Algorithm 2**.

IV. SIMULATION RESULTS

In this section, we demonstrate the performance of the proposed adaptive CSI feedback scheme based on deep equilibrium models for FDD massive MIMO systems.

A. Simulation Setup

1) *Data Generation*: Following the experimental setting in [4], the indoor picocellular scenario working at the 5.3 GHz band is considered. The channel matrices are generated according to the COST 2100 models [16]. The BS is equipped with a uniform linear array with $N_t = 32$ and the number of subcarriers is 1024. The original $2 \times 1024 \times 32$ CSI matrix is transformed into the angular-delay domain and truncated to the first 32 rows, forming the $2 \times 32 \times 32$ matrix \mathbf{H}'' .

2) *Training Settings*: The training, validation, and test datasets contain 100,000, 30,000, and 20,000 samples, respectively. The Adam optimizer is used for trainable weight updates. Kaiming initialization is used for each convolution operation. The numbers of epochs, initial learning rate, and batch size are set as 1000, 0.001, and 20, respectively. The error threshold and maximum iteration number of the limited-memory Broyden's method are set to 0.001 and 20, respectively. The number of groups in group normalization is set to 2. The training loss is the MSE between the recovered CSI and the true CSI. If the training loss does not decrease for 30 epochs, we decrease the learning rate by $1/2$.

3) *Evaluation Metric*: The normalized mean squared error (NMSE) between the recovered channel and the true channel is used to evaluate the performance, which is given by

$$\text{NMSE} = \mathbb{E} \left\{ \frac{\|\mathbf{H}'' - \hat{\mathbf{H}}''\|_2^2}{\|\mathbf{H}''\|_2^2} \right\}. \quad (16)$$

In addition, the number of FLOPs is used to measure the time complexity of the learning model, and the number of trainable parameters is adopted as a metric to measure the space complexity [5]. All the simulations are done using the existing deep learning platform PyTorch. The number of FLOPs and trainable parameters are calculated using the torchstat package for PyTorch.

B. Performance Comparison

To illustrate the effectiveness of the proposed CSI feedback design, we adopt three benchmarks for comparison:

- **CsiNet** [4]: An exploratory work that enjoys low time and space complexity but insufficient reconstruction accuracy.
- **ConvCsiNet** [5]: A complicated CNN-based method achieves good performance but induces heavy computational costs.

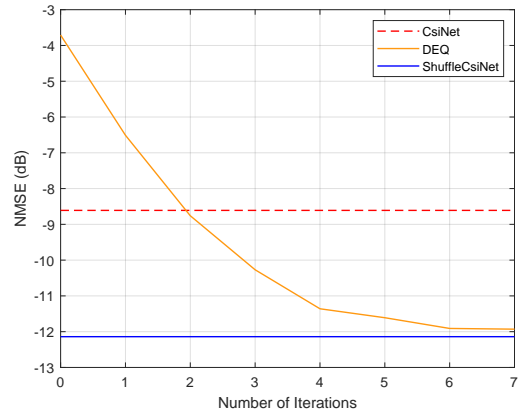


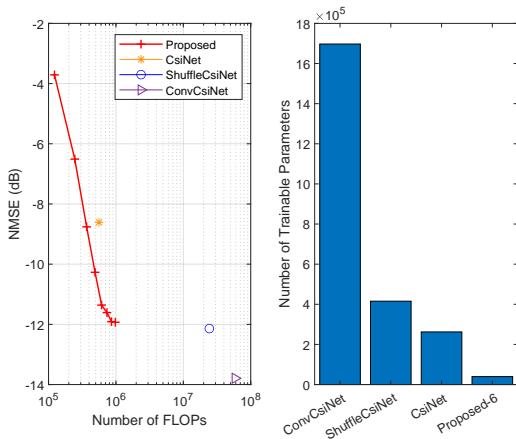
Fig. 3. NMSE achieved by different methods versus the number of iterations when $\gamma = 1/16$.

- **ShuffleCsiNet** [5]: An efficient neural network architecture is adopted, but the complexity is still high for users with extremely limited computational power.

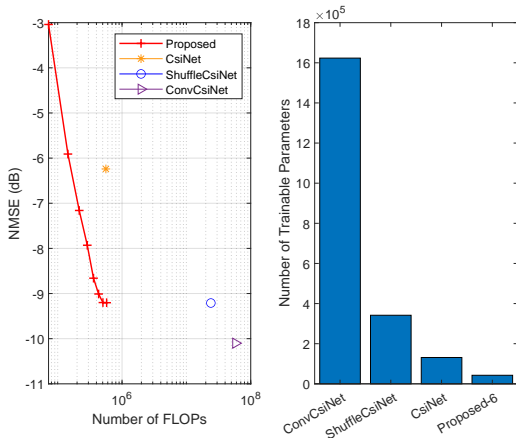
Fig. 3 plots the NMSE achieved by the proposed deep equilibrium learning-based scheme and two other lightweight baselines versus the number of iterations when $\gamma = 1/16$ in the indoor scenario. Since CsiNet and ShuffleCsiNet are explicit neural networks and the outputs are acquired through one time of forward propagation, they do not have the concept of iterations. It can be observed from Fig. 3 that the proposed CSI feedback scheme converges with 6 iterations and achieves a comparable performance with ShuffleCsiNet. Moreover, it is demonstrated that running the proposed method with 2 iterations achieves better performance than CsiNet, showing the superiority of the proposed scheme in terms of efficiency.

In Fig. 4, we demonstrate the accuracy-efficiency trade-offs of different methods. Fig. 4(a) and Fig. 4(b) show the results obtained from $\gamma = 1/16$ and $\gamma = 1/32$ indoor dataset, respectively. From the left subfigures, the NMSE achieved by different methods versus the number of FLOPs at the encoder side is demonstrated. It is shown that although CsiNet only requires a small number of FLOPs and induces low time complexity, the performance is not satisfactory. On the other hand, the ConvCsiNet method achieves around 5 dB higher accuracy compared with CsiNet, but it requires more than 58 million FLOPs. Assume that the compression ratio is $1/16$ and the CSI feedback and recovery period is 1 millisecond. The computational power required by the ConvCsiNet encoder is about 59 G floating point operations per second (FLOPS) [5]. Note that Kirin 970, one of the mid- and high-end mobile systems on chip (SoC), has a total peak computation capability of 244.8 G FLOPS [17]. If the ConvCsiNet is deployed in practice, around $1/4$ of the mobile's computational power is used for CSI feedback, making the other computationally-intensive tasks such as graphics rendering and voice recognition unable to work.

From the left subfigures of Fig. 4, it is demonstrated that the proposed implicit equilibrium model-based CSI feedback scheme provides a better trade-off between accuracy and efficiency. For both $\gamma = 1/16$ and $\gamma = 1/32$, the proposed



(a) $\gamma = 1/16$



(b) $\gamma = 1/32$

Fig. 4. Accuracy-efficiency trade-offs of different methods. (Left) NMSE achieved by different methods versus the number of FLOPs at the encoder side. (Right) The number of trainable parameters of different methods at the encoder side.

scheme achieves the same performance as CsiNet with higher computational efficiency. Besides, after convergence, the performance of the deep equilibrium learning-based approach is comparable with ShuffleCsiNet while the number of FLOPs is greatly reduced. Another advantage of the proposed deep equilibrium learning-based design is that it can achieve an instant accuracy-efficiency trade-off by adjusting the encoder-side equilibrium block iteration number at runtime, while for other baselines, the learning model is fixed once trained.

From the right subfigures of Fig. 4, the numbers of trainable parameters of different methods at the user side are plotted, where Proposed-6 denotes the proposed scheme with 6 iterations for the encoder equilibrium block. Thanks to the weight sharing in the equilibrium block, the number of trainable parameters is greatly reduced, leading to a lower space complexity of the proposed scheme. It is also demonstrated that the ConvCsiNet has the highest space complexity among all the benchmarks. For example, when $\gamma = 1/16$, the ConvCsiNet encoder network needs to store more than 1 million float data, occupying about 6 MB of storage space [5]. In contrast, the

proposed scheme only requires less than 8 thousand float data and thus less than 0.28 MB storage space. This verifies the high efficiency of the proposed CSI feedback scheme.

V. CONCLUSIONS

In this paper, we developed a deep equilibrium learning-based model for CSI feedback in FDD massive MIMO systems. In contrast to existing explicit deep neural networks where multiple layers are cascaded and the neural network output is characterized by successive operations, we utilized a fixed-point equation to specify the input-output relationship. The runtime accuracy-efficiency trade-off can be adjusted according to the resource budget of the users. Extensive simulation results demonstrated that the proposed deep equilibrium learning-based CSI feedback scheme achieves comparable or even better performance with reduced memory and computational cost, when compared with existing lightweight models.

REFERENCES

- [1] F. Boccardi, R. W. Heath, A. Lozano, T. L. Marzetta, and P. Popovski, "Five disruptive technology directions for 5G," *IEEE Commun. Mag.*, vol. 52, no. 2, pp. 74–80, Feb. 2014.
- [2] X. Rao and V. K. N. Lau, "Distributed compressive CSIT estimation and feedback for FDD multi-user massive MIMO systems," *IEEE Trans. Signal Process.*, vol. 62, no. 12, pp. 3261–3271, June 2014.
- [3] J.-C. Shen, J. Zhang, K.-C. Chen, and K. B. Letaief, "High-dimensional CSI acquisition in massive MIMO: Sparsity-inspired approaches," *IEEE Systems Journal*, vol. 11, no. 1, pp. 32–40, Mar. 2017.
- [4] C.-K. Wen, W.-T. Shih, and S. Jin, "Deep learning for massive MIMO CSI feedback," *IEEE Wireless Commun. Lett.*, vol. 7, no. 5, pp. 748–751, Oct. 2018.
- [5] Z. Cao, W.-T. Shih, J. Guo, C.-K. Wen, and S. Jin, "Lightweight convolutional neural networks for CSI feedback in massive MIMO," *IEEE Commun. Letters*, vol. 25, no. 8, pp. 2624–2628, Aug. 2021.
- [6] Y. Cui, A. Guo, and C. Song, "TransNet: Full attention network for CSI feedback in FDD massive MIMO system," *IEEE Wireless Commun. Lett.*, vol. 11, no. 5, pp. 903–907, May 2022.
- [7] S. Bai, J. Z. Kolter, and V. Koltun, "Deep equilibrium models," in *Proc. Advances Neural Inf. Process. Syst.*, vol. 32, Vancouver, Canada, Dec. 2019, pp. 690–701.
- [8] A. Ignatov, R. Timofte, W. Chou, K. Wang, M. Wu, T. Hartley, and L. Van Gool, "AI benchmark: Running deep neural networks on android smartphones," 2018. [Online]. Available: <https://arxiv.org/abs/1810.01109>
- [9] M. Dehghani, S. Gouws, O. Vinyals, J. Uszkoreit, and Ł. Kaiser, "Universal transformers," in *Proc. Int. Conf. Learn. Representations (ICLR)*, New Orleans, USA, May 2019, pp. 1–12.
- [10] W. Yu, Y. Shen, H. He, X. Yu, J. Zhang, and K. B. Letaief, "Hybrid far- and near-field channel estimation for THz ultra-massive MIMO via fixed point networks," in *Proc. IEEE Global Commun. Conf.*, Rio de Janeiro, Brazil, Dec. 2022, pp. 1–6.
- [11] S. Bai, V. Koltun, and J. Z. Kolter, "Multiscale deep equilibrium models," in *Proc. Advances Neural Inf. Process. Syst.*, vol. 33, Dec. 2020, pp. 5238–5250.
- [12] K. He, X. Zhang, S. Ren, and J. Sun, "Deep residual learning for image recognition," in *Proc. IEEE Conf. Comput. Vision Pattern Recognit.*, Las Vegas, USA, 2016, pp. 770–778.
- [13] Y. Wu and K. He, "Group normalization," in *Proc. Eur. Conf. Comput. Vision (ECCV)*, Munich, Germany, Sept. 2018, pp. 3–19.
- [14] K. He, X. Zhang, S. Ren, and J. Sun, "Delving deep into rectifiers: Surpassing human-level performance on imagenet classification," in *Proc. IEEE Int. Conf. Comput. Vision*, Santiago, Chile, Dec. 2015, pp. 1026–1034.
- [15] Y. Zhang, X. Zhang, and Y. Liu, "Deep learning based CSI compression and quantization with high compression ratios in FDD massive MIMO systems," *IEEE Wireless Commun. Lett.*, vol. 10, no. 10, pp. 2101–2105, Oct. 2021.
- [16] L. Liu, C. Oestges, J. Poutanen, K. Haneda, P. Vainikainen, F. Quitin, F. Tufvesson, and P. D. Doncker, "The COST 2100 MIMO channel model," *IEEE Wireless Commun.*, vol. 19, no. 6, pp. 92–99, Dec. 2012.

- [17] S. Wang, A. Pathania, and T. Mitra, "Neural network inference on mobile SoCs," *IEEE Design & Test*, vol. 37, no. 5, pp. 50–57, Jan. 2020.